Density functional perturbation theory with spin-orbit coupling: Phonon band structure of lead

Matthieu J. Verstraete,[1,2,3,*] Marc Torrent,[4] François Jollet,[4] Gilles Zérah,[4] and Xavier Gonze[1,3]
[1]*Unité PCPM and CERMIN, Université Catholique de Louvain, Croix du Sud 1, B-1348 Louvain-la-Neuve, Belgium*
[2]*Physics Department, University of York, Heslington YO10 5DD, United Kingdom*
[3]*European Theoretical Spectroscopical Facility (ETSF), Université Catholique de Louvain, B-1348 Louvain-la-Neuve, Belgium*
[4]*Commissariat à l'Énergie Atomique, F-91680 Bruyères-le-Châtel, France*
(Received 23 April 2008; revised manuscript received 4 June 2008; published 28 July 2008)

The effect of spin-orbit coupling on phonon band structures can be profound for materials containing heavy elements. We describe our implementation of density functional perturbation theory with the spin-orbit interaction for norm-conserving pseudopotentials. We show that the spin-orbit effect on the phonon frequency at the *X* point in face-centered-cubic Pb is very large; it explains the discrepancy between calculated and experimental frequencies previously observed by Liu and Quong [Phys. Rev. B **53**, R7575 (1996)]. Several technical issues (the exchange-correlation functional, the presence of semicore states, the pseudization scheme, and the real-space range of interatomic force constants) are also investigated.

DOI: 10.1103/PhysRevB.78.045119 PACS number(s): 71.15.Mb, 71.70.Ej, 63.20.D−

I. INTRODUCTION

Density functional perturbation theory[1–3] (DFPT) is a widely used method to calculate the response of a system of electrons to an external perturbation. Initially developed as an efficient approach to the treatment of electric fields and atomic vibrations[4,5] within density functional theory (DFT), the method has been generalized for many other types of perturbations such as applied strains,[6,7] alchemical perturbation[8] (changing the nature of an atomic species), magnetic field,[9,10] or to compute more involved material properties such as superconducting and transport coefficients,[11] thermodynamic properties[12] including thermal expansion,[13] or higher-order (nonlinear) responses, such as Raman intensities[14,15] or electro-optic coupling.[16,17]

In this paper, we present a DFPT implementation for vibrational properties that includes the spin-orbit (SO) interaction, a relativistic effect. Formally the SO effect is always present and gives corrections to the total energy and its derivatives. Actually, the strength of the SO coupling increases quickly with the atomic number *Z*: as inner-shell electrons are pulled closer to the nucleus, their kinetic energy increases and relativistic effects become very important. In many cases, for light elements, these can be neglected or approximated by the scalar-relativistic terms in the Dirac equation.[18] However, for specific properties, SO effects might be important even when only light elements are present, as for graphite.[19] In second-row transition metals and heavier elements, but also for some lighter elements, the SO effect is essential to reproduce correctly the *electronic* structure of materials. Classic examples include the valence-band splitting of GaAs (Ref. 20) and the multiplet structure of the *f*-band metals.[21] For heavier elements, in general, the SO effect becomes as important for *structural* and *dynamical* properties as for electronic properties.

We will consider the common norm-conserving pseudopotential approximation, which "freezes out" the core electrons, replacing their effect on the valence electrons with a (usually nonlocal) pseudopotential operator. In this approach the SO effect is contained in modified pseudopotentials which depend on the spinorial state of an electron, which can be factored out explicitly as a $\mathbf{L}\cdot\mathbf{S}$ term.[22] The application of such a term on spinor wave function can be done on the basis of spherical harmonics, as described in Ref. 23, or on Legendre functions, as outlined in Ref. 24. In both cases, the modifications to be applied to the DFPT treatment for phonons (atomic displacements) are particularly simple, as will become apparent in the present paper. Indeed the atomic displacements do not modify the pseudopotential, but only the structure factor governing the contribution of each pseudopotential to total potential. We will always consider in the following that the pseudopotential is separable, as in the construction of Kleinman and Bylander.[25]

The SO coupling within DFT and DFPT, norm-conserving pseudopotentials and plane waves, has been implemented by some of us (2001–2002) in the ABINIT software package (Version 3.1).[24,26] It has been used for several phonon-based studies: thorium,[27] bismuth[28–30] including bismuth specific heat,[31] and for the first full phonon band structure of uranium.[32] In Ref. 30, the phonon band structure of bismuth has been specifically investigated with and without the SO interaction, isolating the direct effect due to the modification of the dynamical matrix at fixed crystallographic parameters from the indirect effect arising from the change in crystallographic parameters. The inclusion of the spin-orbit coupling modified the phonon frequencies by 10–20% throughout the whole Brillouin zone (BZ). Most of the modifications were due to the direct effect, except for the acoustic mode frequencies along the $\Gamma-T$ line, for which the indirect effect dominated.

A formalism for inclusion of SO in ultrasoft pseudopotentials (USPP)[33] has recently been presented by Dal Corso and Mosca Conte.[34,35] They examined the phonon band structures of Au and Pt. In both cases, the SO had an effect much smaller than in bismuth on the order of 1%.

In the present paper, after a brief presentation of the DFPT formalism for computing phonons (Sec. II), we describe our formalism (Sec. III), which is simpler than the ultrasoft pseudopotential case. Because we have tested several approximations within DFT (see below), Sec. IV focuses on the pseudopotential generation procedure. We then con-

tinue by examining the effect of SO on the phonon band structure of Pb (Sec. V). Like Bi, the Pb atom has an incomplete $6p$ shell, which is strongly affected by the SO interaction ($6p_{1/2}-6p_{3/2}$ splitting on the order of 1 eV). By contrast, Au and Pt expose a $6s$ incomplete shell or a filled $5d$ shell, which exhibit smaller changes in bonding or dynamical matrices due to the SO coupling. We will show that for Pb the SO induces a modification of some phonon frequencies at X by as much as 60%. In the remainder of the Brillouin zone, the modification of the phonon frequencies is smaller than in bismuth, but still on the order of 5%–10%, and much larger than for Au or Pt.

We consider different technical issues, not questioned in previous studies. We base our study mainly on pseudopotentials of the Troullier and Martins[36] (TM) flavor (made fully separable, thanks to the Kleinman and Bylander transformation[25]), with some comparison with Hartwigsen-Goedecker-Hutter (HGH) pseudopotentials[22] when appropriate. We have examined the effects of the exchange-correlation (XC) functional [the generalized gradient approximation (GGA) for the TM pseudopotential and the local density approximation (LDA)] and of the $5d$ electrons (treated as semicore states explicitly included in the self-consistent treatment or treated as core states).

II. DENSITY FUNCTIONAL PERTURBATION THEORY

DFPT builds on the calculation in DFT (Refs. 37 and 38) of the total energy of a system of electrons in a given external potential. It calculates the derivatives of the total energy with respect to different perturbations of the potential (e.g., an electric field, atomic displacement, and strain). DFPT for phonons was reviewed comprehensively by Baroni *et al.*[4] In this section we summarize the elements of DFPT we will need and introduce standard notation used in Refs. 2 and 3.

If the strength of the perturbation is characterized by a parameter λ, then the energy, potentials, and wave functions have an expansion as a function of that parameter. The energy reads

$$E = E^{(0)} + \lambda E^{(1)} + \lambda^2 E^{(2)} + \cdots . \tag{1}$$

The forces and stresses are first-order derivatives of the energy (contained in $E^{(1)}$) with respect to the appropriate perturbation (atomic displacement or strain). Many experiments, such as Raman and infrared spectroscopies, linear optics, and elastic constants measurements, probe $E^{(2)}$. The major step in obtaining $E^{(2)}$ is the computation of the first-order change in wave functions $\psi^{(1)}$, derived either from a variational principle for $E^{(2)}$ (see Ref. 39) or from a Sternheimer equation,[40]

$$P_c(H^{(0)} - \epsilon_n^{(0)})|\psi_n^{(1)}\rangle = -P_c H^{(1)}|\psi_n^{(0)}\rangle, \tag{2}$$

where P_c is the projector on the conduction bands, $\epsilon_n^{(0)}$ and $\psi_n^{(0)}$ the ground-state eigenenergies and eigenfunctions, and $H^{(1)}$ the first-order perturbed Hamiltonian. The knowledge of $\psi^{(1)}$ is also the major step in the computation of $E^{(3)}$, thanks to the so-called "$2n+1$," applied to DFT.[41]

The perturbation often has a directional dependence, described by a vector $\vec{q}$ in reciprocal space. This could be the wave vector of an electric field or of a phonon (see below). The most primitive approach to calculating a perturbation (without perturbation theory) is to freeze a finite perturbation into the system and to calculate the energies for different values of λ in order to numerically extract the derivatives. This method is known as the frozen-phonon technique for atomic perturbations. Calculating a frozen phonon for $\vec{q} \neq 0$ requires a supercell to describe the full fluctuation of the perturbation [which is modulated by $\exp(-i\vec{q}\vec{r})$]. As a result calculations become unwieldy for small or unsymmetrical $\vec{q}$ vectors and are impossible if $\vec{q}$ is not commensurate with the reciprocal lattice. DFPT does not suffer from this drawback and can be used with arbitrary $\vec{q}$. It must be noted that for the specific $\vec{q}=0$ the calculational weight of the frozen-phonon technique can be comparable to that of DFPT and that the finite perturbation method then has the advantage of giving access to higher-order responses without involved formalism or time-consuming implementation.

The presence of the SO coupling will not modify profoundly the above-mentioned equations. A first difference will come from the replacement of scalar wave functions $\psi_n^{(0)}$ and $\psi_n^{(1)}$ by spinor wave functions $\psi_{n,\sigma}^{(0)}$ and $\psi_{n,\sigma}^{(1)}$. Then, an additional SO term will be present in the $H^{(0)}$ and $H^{(1)}$ terms of the Sternheimer equation,[40] and finally, there will be a direct (frozen-wave-function) contribution to the second-order derivative of the total energy $E^{(2)}$. The Hamiltonian and energy modifications will be described in Sec. III.

In the case of phonons, one wants to calculate all the second derivatives of E with respect to the displacements of two atoms. This derivative gives the interatomic force constants (IFC),[42] which can be understood as the change in the force on one atom if another atom is displaced from its original position. The IFC can be defined as

$$C_{\kappa\alpha;\kappa'\beta}(a,b) = \frac{\partial^2 E}{\partial R^a_{\kappa\alpha}\, \partial R^b_{\kappa'\beta}}, \tag{3}$$

where a and b label unit cells, κ and κ' label atoms in the unit cells, and α and β label the reduced directions in which the atoms are displaced. The atomic positions are $\vec{R}^a_\kappa$ and $\vec{R}^b_{\kappa'}$. In many systems, the IFC die off slowly with the distance between the atoms; the movement of an atom can influence the force on an atom many cells away.[43]

The Fourier transform (FT) of $C_{\kappa\alpha;\kappa'\beta}(a,b)$ with respect to the cell lattice positions a and b gives the dynamical matrix $\tilde{D}_{\kappa\alpha;\kappa'\beta}(\vec{q})$ (with an additional factor of $1/\sqrt{M_\kappa M_{\kappa'}}$). Diagonalizing $\tilde{D}$ gives eigenvalues, which are the square of the phonon frequencies $\omega^2_{m\vec{q}}$, and the phonon polarization vectors. If $\vec{q}=0$ one can compare the frequencies to Raman and infrared frequencies, and the full phonon band structure can be obtained from different techniques, such as inelastic x-ray scattering.

III. INCLUSION OF THE SPIN-ORBIT INTERACTION IN DFPT

The inclusion of the full Dirac equation in an all-electron framework is technically difficult, and most calculations are performed at the spin-orbit coupling level, that is, they are

accurate to order $Z^2\alpha^2$. In contrast, as has been shown a long time ago by Kleinman,[44] in the pseudopotential framework the Dirac equation is pseudized as a Pauli-type equation, which is then accurate up to order α^2.

A. Spin-orbit coupling in the plane-wave basis context

In a fully relativistic separable pseudopotential approach, the spin-orbit coupling term appears only in the electron-ion potential. In our case the potential has the form[45] (for a single atom system)

$$V_{ei}(\mathbf{r},\mathbf{r}') = \sum_l V_l^{\mathrm{SR}}(r,r')|ls\rangle\langle ls| + \sum_l V_l^{\mathrm{SO}}(r,r')\mathbf{L}\cdot\mathbf{S}|ls\rangle\langle ls|, \tag{4}$$

where $|ls\rangle\langle ls|$ is the projector on the tensor product $L\otimes S$ [dimension of $2(2l+1)$] of functions of a given angular momentum times the spin space. The terms $V_l^{\mathrm{SR}}(r,r')$ or $V_l^{\mathrm{SO}}(r,r')$ are spin independent potential parts which we assume separable, as in the construction of Kleinman and Bylander[25] (for sake of simplicity, we suppose only one projector per angular-momentum channel),

$$V_l^x(r,r') = f_l^x(r)E_l^{\mathrm{KB},x}f_l^x(r'), \tag{5}$$

where $E_l^{\mathrm{KB},x}$ is the Kleinman-Bylander energy[46] and x is either SO or SR (for scalar relativistic).

The HGH pseudopotentials[22] are fully relativistic pseudopotentials directly available within this formulation. The transformation that must be done to obtain such a formulation for Troullier-Martins pseudopotentials[36] is explained in Appendix A.

In each $|ls\rangle$ space, the $V_l^{\mathrm{SR}}(r,r')$ or $V_l^{\mathrm{SO}}(r,r')$ and $\mathbf{L}\cdot\mathbf{S}$ operators commute, so the order of operations is irrelevant. Indeed, in many texts, the projector is not explicitly written.

The standard plane-wave basis is extended to the spinor plane-wave basis, whose elements are two component plane waves denoted by $\langle\mathbf{G},\sigma|$. A generic matrix element takes the forms

$$\mathbf{V}_l^{\mathrm{SR}}(\mathbf{G}\sigma,\mathbf{G}'\sigma') = \langle\mathbf{G},\sigma|V_l^{\mathrm{SR}}|l,s\rangle\langle l,s|\mathbf{G}',\sigma'\rangle \tag{6}$$

for the scalar-relativistic part and

$$\mathbf{V}_l^{\mathrm{SO}}(\mathbf{G}\sigma,\mathbf{G}'\sigma') = \langle\mathbf{G},\sigma|V_l^{\mathrm{SO}}\mathbf{L}\cdot\mathbf{S}|l,s\rangle\langle l,s|\mathbf{G}',\sigma'\rangle \tag{7}$$

for the spin-orbit part.

The result for the scalar-relativistic part is well known,[25]

$$\mathbf{V}_l^{\mathrm{SR}}(\mathbf{G}\sigma,\mathbf{G}'\sigma') = \frac{4\pi}{\Omega}(2l+1)\delta_{\sigma\sigma'}E_l^{\mathrm{KB,SR}} \times P_l(\hat{G}\cdot\hat{G}')f_l^{\mathrm{SR}}(G)f_l^{\mathrm{SR}}(G'), \tag{8}$$

where $\hat{G}=\frac{\mathbf{G}}{|G|}$, $G=|\mathbf{G}|$, and $f_l^{\mathrm{SR}}(G)=\int_0^\infty f_l^{\mathrm{SR}}(r)j_l(Gr)r^2dr$. j_l is a spherical Bessel function and P_l is a Legendre polynomial. This results from the addition theorem, which states

$$\langle\mathbf{G}|l,s\rangle\langle l,s|\mathbf{G}'\rangle = \sum_m \langle\mathbf{G}|Y_{lm}^*Y_{lm}|\mathbf{G}'\rangle = \frac{(2l+1)}{4\pi}P_l(\hat{G}\cdot\hat{G}'). \tag{9}$$

To achieve an analog formula for the spin-orbit term, we first consider the vector $\mathbf{L}|\mathbf{G}'\rangle$. Using the definition $\mathbf{L}=\mathbf{r}\times\mathbf{p}$ and the identity $\mathbf{p}|\mathbf{G}'\rangle=\mathbf{G}'|\mathbf{G}'\rangle$, we obtain $\mathbf{L}|\mathbf{G}'\rangle=-i\mathbf{G}'\times\nabla_{\mathbf{G}'}|\mathbf{G}'\rangle$. We therefore transform the matrix element [Eq. (7)] in

$$\mathbf{V}_l^{\mathrm{SO}}(\mathbf{G}\sigma,\mathbf{G}'\sigma') = -i\langle\sigma|\mathbf{S}|\sigma'\rangle\cdot\mathbf{G}'\times\nabla_{\mathbf{G}'}\langle\mathbf{G}|V_l^{\mathrm{SO}}|l,s\rangle\langle l,s|\mathbf{G}'\rangle. \tag{10}$$

Noting that the $\nabla_{\mathbf{G}'}(|\mathbf{G}'|)$ terms do not contribute, due to the cross product with $\mathbf{G}'$, we finally obtain

$$\mathbf{V}_l^{\mathrm{SO}}(\mathbf{G}\sigma,\mathbf{G}'\sigma') = -i\frac{4\pi}{\Omega}(2l+1)E_l^{\mathrm{KB,SO}} \times P_l'(\hat{G}\cdot\hat{G}')f_l^{\mathrm{SO}}(G)f_l^{\mathrm{SO}}(G') \times\left(\langle\sigma|\mathbf{S}|\sigma'\rangle\cdot\frac{\mathbf{G}\times\mathbf{G}'}{GG'}\right), \tag{11}$$

where P_l' is the first derivative of P_l and $\mathbf{S}$ the spin operator represented by the Pauli matrices.

Although perfectly analogous in principle, the inclusion of relativistic effects in the USPP case is much more involved (see Refs. 34 and 35). The equivalent of the Kleinman-Bylander energies (usually called D) become matrices as a function of l. The augmentation functions, overlap matrices, and D all acquire terms due to spin-orbit interactions.

B. Spin-orbit coupling and phonons

In the case of a system containing several atoms κ, the previous nonlocal matrix elements can be expressed by the simple inclusion of structure factors in a sum over ionic positions $\mathbf{R}_\kappa$. The scalar-relativistic part becomes

$$\mathbf{V}_l^{\mathrm{SR}}(\mathbf{G}\sigma,\mathbf{G}'\sigma') = \frac{4\pi}{\Omega}(2l+1)\delta_{\sigma\sigma'}\sum_\kappa E_{\kappa,l}^{\mathrm{KB,SR}}P_l(\hat{G}\cdot\hat{G}')f_{\kappa,l}^{\mathrm{SR}}(G)f_{\kappa,l}^{\mathrm{SR}}(G')e^{i(\mathbf{G}'-\mathbf{G})\mathbf{R}_\kappa}. \tag{12}$$

Similarly, the spin-orbit part becomes

$$\mathbf{V}_l^{\mathrm{SO}}(\mathbf{G}\sigma,\mathbf{G}'\sigma') = -i\frac{4\pi}{\Omega}(2l+1)\sum_\kappa E_{\kappa,l}^{\mathrm{KB,SO}}P_l'(\hat{G}\cdot\hat{G}')f_{\kappa,l}^{\mathrm{SO}}(G)f_{\kappa,l}^{\mathrm{SO}}(G')\left(\langle\sigma|\mathbf{S}|\sigma'\rangle\cdot\frac{\mathbf{G}\times\mathbf{G}'}{GG'}\right)e^{i(\mathbf{G}'-\mathbf{G})\mathbf{R}_\kappa}. \tag{13}$$

As emphasized in Sec. II the determination of phonon frequencies involves the first-order perturbed Hamiltonian due to an atomic displacement as well as the second derivative of E with respect to the displacements of two atoms.[2,3] As spin-orbit coupling is only involved in the separable nonlocal term of Hamiltonian, the only impacted terms are $\langle\psi_n^{(0)}|\frac{\partial^2 V_{ei}}{\partial R_{\kappa\alpha}\partial R_{\kappa'\beta}}|\psi_n^{(0)}\rangle$ and $\frac{\partial V_{ei}}{\partial R_{\kappa\alpha}}|\psi_n^{(1)}\rangle$.

The expressions for these two terms are rather simple because atomic displacements do not modify the pseudopotential but only the structure factors. They are directly connected with the following derivatives:

$$\langle \mathbf{G}\sigma|\frac{\partial \mathbf{V}_l^{\mathrm{SR}}}{\partial R_{\kappa\alpha}}|\psi_{n\sigma'}^{(1)}\rangle = i\frac{4\pi}{\Omega}\delta_{\sigma\sigma'}(2l+1)E_{\kappa,l}^{\mathrm{KB,SR}}\sum_{\mathbf{G}'}P_l(\hat{G}\cdot\hat{G}')f_{\kappa,l}^{\mathrm{SR}}(G)f_{\kappa,l}^{\mathrm{SR}}(G')c_{n\sigma'}^{(1)}(\mathbf{G}')(G'_\alpha - G_\alpha)e^{i(\mathbf{G}'-\mathbf{G})\mathbf{R}_\kappa}, \tag{14}$$

$$\langle \mathbf{G}\sigma|\frac{\partial \mathbf{V}_l^{\mathrm{SO}}}{\partial R_{\kappa\alpha}}|\psi_{n\sigma'}^{(1)}\rangle = \frac{4\pi}{\Omega}(2l+1)E_{\kappa,l}^{\mathrm{KB,SO}}\sum_{\mathbf{G}'}\left(\langle\sigma|\mathbf{S}|\sigma'\rangle\cdot\frac{\mathbf{G}\times\mathbf{G}'}{GG'}\right)P_l'(\hat{G}\cdot\hat{G}')f_{\kappa,l}^{\mathrm{SO}}(G)f_{\kappa,l}^{\mathrm{SO}}(G')c_{n\sigma'}^{(1)}(\mathbf{G}')(G'_\alpha - G_\alpha)e^{i(\mathbf{G}'-\mathbf{G})\mathbf{R}_\kappa}, \tag{15}$$

$$\begin{aligned}\frac{\partial^2 E_{ei}^{\mathrm{SR}}}{\partial R_{\kappa\alpha}\partial R_{\kappa\beta}} &= \sum_{n,l,\sigma,\sigma'} f_n\langle\psi_{n\sigma}^{(0)}|\frac{\partial^2 \mathbf{V}_l^{\mathrm{SR}}}{\partial R_{\kappa\alpha}\partial R_{\kappa\beta}}|\psi_{n\sigma'}^{(0)}\rangle \\ &= -\frac{4\pi}{\Omega}\sum_{n,l} f_n(2l+1)E_{\kappa,l}^{\mathrm{KB,SR}}\sum_{\mathbf{G}\sigma,\mathbf{G}'\sigma'}\delta_{\sigma\sigma'}P_l(\hat{G}\cdot\hat{G}')f_{\kappa,l}^{\mathrm{SR}}(G)f_{\kappa,l}^{\mathrm{SR}}(G')2\Re[(G'_\alpha - G_\alpha)G'_\beta e^{i(\mathbf{G}'-\mathbf{G})\mathbf{R}_\kappa}c_{n\sigma}^{(0)*}(\mathbf{G})c_{n\sigma'}^{(0)}(\mathbf{G}')],\end{aligned} \tag{16}$$

$$\begin{aligned}\frac{\partial^2 E_{ei}^{\mathrm{SO}}}{\partial R_{\kappa\alpha}\partial R_{\kappa\beta}} &= \sum_{n,l,\sigma,\sigma'} f_n\langle\psi_{n\sigma}^{(0)}|\frac{\partial^2 \mathbf{V}_l^{\mathrm{SO}}}{\partial R_{\kappa\alpha}\partial R_{\kappa\beta}}|\psi_{n\sigma'}^{(0)}\rangle \\ &= i\frac{4\pi}{\Omega}\sum_{n,l} f_n(2l+1)E_{\kappa,l}^{\mathrm{KB,SO}}\sum_{\mathbf{G}\sigma,\mathbf{G}'\sigma'}P_l'(\hat{G}\cdot\hat{G}')f_{\kappa,l}^{\mathrm{SO}}(G)f_{\kappa,l}^{\mathrm{SO}}(G')\left(\langle\sigma|\mathbf{S}|\sigma'\rangle\cdot\frac{\mathbf{G}\times\mathbf{G}'}{GG'}\right) \\ &\quad\times 2\Re[(G'_\alpha - G_\alpha)G'_\beta e^{i(\mathbf{G}'-\mathbf{G})\mathbf{R}_\kappa}c_{n\sigma}^{(0)*}(\mathbf{G})c_{n\sigma'}^{(0)}(\mathbf{G}')].\end{aligned} \tag{17}$$

$|\psi_{n\sigma}^{(0)}\rangle$ ($|\psi_{n\sigma}^{(1)}\rangle$) is a spinorial component of wave function $\psi_n^{(0)}$ (first-order wave function $\psi_n^{(1)}$). f_n is the occupation number and $c_{n\sigma}^{(0)}(\mathbf{G})$ and $c_{n\sigma}^{(1)}(\mathbf{G})$ are plane-wave coefficients.

IV. CONSTRUCTION OF THE PSEUDOPOTENTIALS

A number of different variables must be considered in the construction of our TM pseudopotential. Linear response quantities are more delicate to access and converge than the ground state, and careful consideration is needed; we must choose which electrons will be treated explicitly as valence in the self-consistent run, which level of relativistic approximation we will use (scalar relativistic or full spin orbit), and which XC functional will be employed [the LDA (Ref. 38) or Perdew-Burke-Ernzerhof (PBE)-GGA (Ref. 47) in our study]. Our main result, namely, the noticeable effect of SO on phonon frequencies, especially at the X point (see Sec. V), is unaffected by these despite some fluctuations.

We have generated eight TM pseudopotentials: with and without SO, with and without semicore $5d$ electrons, and using LDA or GGA. The pseudopotential matching radius was set to 1.7 bohr in all cases. For the ground-state properties, the semicore electrons have little effect, which could have been expected in this homogeneous system. The LDA TM potential strongly underestimates the experimental volume (109 Å^3 instead of 121 Å^3). Worse, it predicts the wrong phase ordering: the diamond phase is lower in energy than fcc. The SO interaction does not affect the structure strongly, but we will see below that the electronic and vibrational properties change substantially. Comparison with structural and vibrational data shows that the best result is obtained with the most complete pseudopotential: GGA with semicore and with SO interaction.

The relaxed lattice parameter with the GGA SO $5d$ pseudopotential is 4.958 Å, in excellent agreement with the experimental value of 4.951 Å. The presence of semicore states necessitates a fairly high kinetic-energy cutoff of 30 Ha, which we use for the other TM potentials as well. We have performed all phonon band-structure calculations at the correspondingly relaxed lattice parameters, given in Table I. The largest difference is between LDA and GGA for the TM cases. The SO coupling has almost no effect on the volume. The inclusion of semicore states has an effect for the LDA case.

To verify whether the LDA approximation itself is in question, we have also tested another type of pseudopotential which incorporates SO interaction, of the HGH (Ref. 22) flavor, which converges with a plane-wave cutoff of 16 Ha.

TABLE I. Comparison of lattice parameters in LDA and GGA, with and without the SO interaction and with and without the semicore (SC) 5*d* electrons treated as valence electrons. In the first column of numerical values the reference is presented (in Å): a GGA Troullier-Martins pseudopotential (Ref. 36) with semicore electrons. The other columns give the percent change with respect to this reference. The HGH column refers to HGH pseudopotentials, with LDA and no semicore electrons.

Reference, Å (GGA SC SO)		GGA SC	LDA SC	GGA	LDA	HGH
4.958	SO	0%	−3.4%	−0.2%	−4.8%	−2.3%
	No SO	−0.2%	−3.5%	−0.3%	−4.8%	−2.4%

The HGH published parametrization has no semicore electrons, but we have seen above that the semicore has a rather small effect, and the same is true for the phonons below. The HGH LDA pseudopotential predicts the correct ordering of the diamond and fcc phases and yields a better lattice parameter of 4.84 Å (volume of 113 $Å^3$). The worse quality of the LDA TM potential is thus not due exclusively to the LDA but to the combination of the TM scheme with LDA volume underestimation. It is the absence of semicore electrons which allows for convergence with a lower plane-wave cutoff than the TM pseudopotential. In the following we will focus mainly on the reference GGA TM pseudopotential with semicore electrons.

V. EFFECT OF SPIN ORBIT ON PHONONS IN fcc LEAD

The phonon band structure of lead was calculated as one of the first applications of DFPT to metals and broadly gave good agreement[11,49] except at the *X* point. It was suggested in Ref. 49 that the discrepancies could be due to the lack of spin-orbit coupling. This is indeed the case: in Fig. 1 we show the phonon-dispersion curves for fcc Pb with and without the spin-orbit effect compared to experiment. The phonon modes at many $\vec{q}$ change appreciably with the SO effect, but at the *X* point the effect is dramatic, and the *X* transverse frequency softens by more than 10 cm^{-1}. As a whole the lowest branch is the most affected. Also the highest branch is largely affected along the $\Gamma-K$ and $\Gamma-L$ directions.

The Fermi surface (FS) of lead is quite complicated, with small pockets of electrons and holes, and it is necessary to sample the electronic and vibrational degrees of freedom in the Brillouin zone with at least a $12\times12\times12$ Monkhorst-Pack[50] grid [72 *q* points in the irreducible Brillouin zone (IBZ)]. This dense grid was necessary to resolve the Kohn anomalies and nonsinusoidal behavior of the phonon bands. We examined this effect, in the case of the HGH (Ref. 22) pseudopotentials, using even better Monkhorst pack grids, up to a $32\times32\times32$ grid (897 *k* points in the IBZ) for the electronic degrees of freedom. In this case we relied on a somewhat coarser $8\times8\times8$ BZ sampling (29 *q* points in the IBZ) for the vibrational degrees of freedom, thanks to the approximation scheme presented in Appendix B, using a cutoff of the IFC in real space. These details of the scheme are presented because it is simple and may be of interest for other implementations of DFT phonon calculations (the cutoff was *only* used for the comparison calculations using the HGH pseudopotential). It remains, however, quite a severe approximation (neglecting slowly converging long-range IFC), which must be used with care. In this way, reducing the sampling of vibrational degrees of freedom from $12\times12\times12$ to $8\times8\times8$ does not affect the precision of the phonon frequencies.

The phonon frequencies calculated with the different pseudopotentials are compared in Table II for selected high-symmetry points. The effect of the SO interaction is remarkably strong, almost halving the frequencies at the *X* point, and softening the transverse modes at *K* and *L* as well. The longitudinal modes are much less sensitive to the SO effect.

As we explained in Ref. 51 for monoatomic wires of Pb, the SO interaction has the effect of shifting part of the Fermi surface to a $\vec{k}$ point which gives a Kohn anomaly[52] at $2k_F = X$. The electronic effect is similar but more subtle in three-dimensional (3D) bulk Pb, as can be seen from the compari-

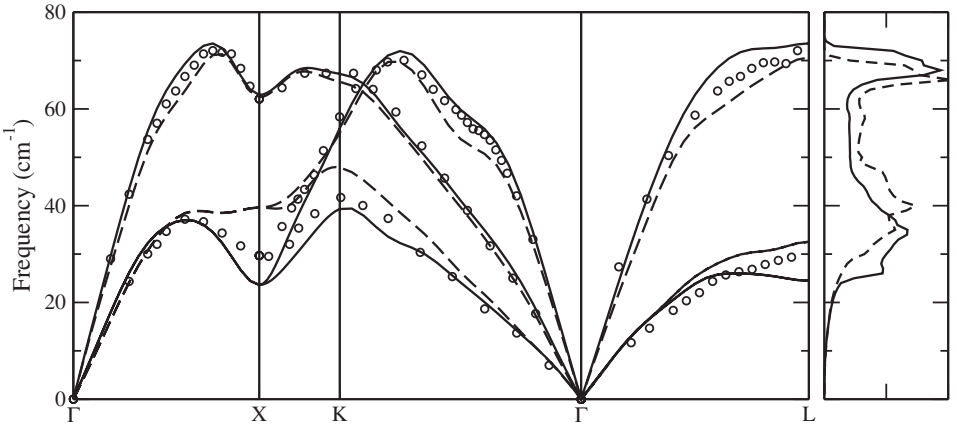

FIG. 1. The phonon band structure of lead, with (solid) and without (dashed) spin-orbit interaction. The circles are experimental data from Ref. 48. Note the dramatic effect of SO for the lowest branch around *X* and *K*. Side panel: phonon density of states with (solid line) and without (dashed) SO coupling.

TABLE II. Comparison of phonon frequencies with different pseudopotentials, with and without the SO interaction. Columns and notation as in Table I. The GGA reference is presented (in cm^{-1}). The LDA/GGA difference is relatively constant, and the effect of spin-orbit coupling is very strong, particularly for the TA mode at *X*.

Phonon mode	Reference, cm^{-1} (GGA SC SO)	Spin-orbit treatment	GGA SC relative diff.	LDA SC relative diff.	GGA relative diff.	LDA relative diff.	HGH relative diff.
X TA	23.6	SO	0%	6%	26%	23%	19%
		No SO	68%	74%	84%	73%	65%
X LA	62.9	SO	0%	18%	−7%	7%	1%
		No SO	−1%	14%	7%	15%	6%
K TA	39.3	SO	0%	7%	7%	16%	1%
		No SO	22%	29%	29%	32%	5%
K LA	67.3	SO	0%	12%	−4%	6%	−3%
		No SO	−3%	8%	4%	11%	−6%
L TA	24.5	SO	0%	8%	23%	33%	22%
		No SO	33%	37%	42%	41%	30%
K LA	67.3	SO	0%	12%	−4%	6%	−3%
		No SO	−3%	8%	4%	11%	−6%
L LA	73.6	SO	0%	16%	−6%	9%	−6%
		No SO	−4%	10%	1%	13%	4%

son of the electronic band structures with and without SO in Fig. 2. The change in the bands at the Fermi level is quite small, but around the *W* point the bands nearest to E_F are affected. Doubling the *W k* point brings us to a wave vector which folds back to *X*.

In Table II we also compare phonon frequencies for the potential with and without semicore *d* electrons and for different XC approximations. The results depend more on the inclusion of the SO effect than on the XC method. The presence of the *d* states does not modify the results strongly, and in particular the LDA HGH frequencies are very close to the GGA TM ones. Overall, we can say that potentials which produce good ground-state structural data also give good vibrational properties, and in any case, the effect of SO, as deduced from the GGA TM case with semicore states, is confirmed, despite some fluctuations, which are to be expected from the differing constructions of the norm-conserving pseudopotentials.

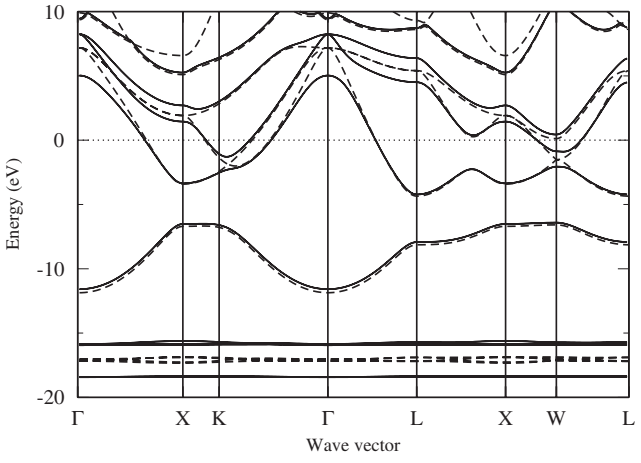

FIG. 2. The electronic band structure of lead (in eV), with (solid) and without (dashed) spin-orbit interaction. The Fermi level is at 0.

VI. CONCLUSIONS

We have laid to rest an important discrepancy in the phonons of Pb, which had been recognized over ten years ago.[49] The phonon band structure of face-centered-cubic lead is profoundly affected by the inclusion of the spin-orbit interaction.

We have shown how this interaction can be incorporated into norm-conserving pseudopotential based DFPT calculations of dynamical matrices and phonon frequencies. The nature of the pseudopotential also affects the phonon band structure, but to a lesser extent, through the construction scheme, the approximation used for the exchange-correlation functional, and the relaxed lattice parameter. The presence or the absence of the 5*d* states in the set of valence electrons does not alter strongly the electronic or vibrational properties of pure lead; this was expected as the *d* electrons are quite inert, 4.6 eV below the *s* bands, and the *d* shell is always filled in elemental Pb.

The method exposed here has opened the possibility of accurately simulating the vibrational properties of heavy atoms, including *d* and *f* row elements, as witnessed by several previous phonon band-structure calculations including SO interaction. The further inclusion of SO with strong correlation methods, such as LDA+*U*, in phonon calculations, must be considered in order to complete the accurate description of heavier elements. Some work in this direction has begun[53] but much remains to be done, in particular in application to efficient DFPT methods.

Finally, the somewhat fluctuating behavior and quality shown for different combinations of pseudopotential scheme and XC approximation combinations call for more precise

methodologies to calculate phonon frequencies. For the ultrasoft scheme, the implementation of SO within DFPT has been published.[35] The DFPT implementation of the projector augmented wave (PAW) formalism[54,55] should be complemented by taking into account SO effects.

ACKNOWLEDGMENTS

This research has been supported by the Belgian FRFC (Project No. 2.4502.05), the ARC "Interaction Électron–Vibration dans les Nanostructures," the Interuniversity Attraction Poles Program (Grant No. P6/42), Belgian State, Belgian Science Policy, the EU's Sixth Framework Programme though the NANOQUANTA EU Network of Excellence (Grant No. NMP4-CT-2004-500198), a Marie Curie Intra-European Fellowship (Grant No. MEIF-CT-2005-024152), and the EU's Seventh Framework Programme though the ETSF I3 e-Infrastructure project (Grant Agreement No. 211956).

APPENDIX A: DESCRIPTION OF THE TREATMENT OF SPIN-ORBIT COUPLING IN THE CASE OF TROULLIER-MARTINS PSEUDOPOTENTIALS

In the case of norm-conserving Troullier-Martins pseudopotentials,[36] the nonlocal pseudopotential can be written[56] as

$$V_{\mathrm{NL}} = \sum_l |ls\rangle(|v_l^{\mathrm{ion}}\rangle\langle v_l^{\mathrm{ion}}|)\langle ls| + \sum_l |ls\rangle(|v_l^{\mathrm{ion}}\rangle\langle v_l^{\mathrm{SO}}| + |v_l^{\mathrm{SO}}\rangle\langle v_l^{\mathrm{ion}}|)\mathbf{L}\cdot\mathbf{S}\langle ls| + \sum_l |ls\rangle\left(|v_l^{\mathrm{SO}}\rangle\left(\frac{1}{4}l(l+1) - \frac{1}{2}\mathbf{L}\cdot\mathbf{S}\right)\langle v_l^{\mathrm{SO}}|\right)\langle ls| \tag{A1}$$

with the same notations as in Ref. 56 (we assume that the Kleinman-Bylander energy factors have been absorbed in the definition of v_l^{ion} and v_l^{SO}),

$$v_l^{\mathrm{ion}} = \frac{1}{(2l+1)}[(l+1)v_{l,l+1/2} + (l)v_{l,l-1/2}], \tag{A2}$$

$$v_l^{\mathrm{SO}} = \frac{2}{(2l+1)}[(v_{l,l+1/2} - v_{l,l-1/2}\ ], \tag{A3}$$

where $v_{l,l+1/2}$ and $v_{l,l-1/2}$ are the lj components of a pseudopotential coming from the resolution of the Dirac equation.

This can be rewritten as

$$V_{\mathrm{NL}} = \sum_l |ls\rangle\left(|v_l^{\mathrm{ion}}\rangle\langle v_l^{\mathrm{ion}}| + |v_l^{\mathrm{SO}}\rangle\frac{1}{4}l(l+1)\langle v_l^{\mathrm{SO}}|\right)\langle ls| + \sum_l \langle ls| \times\left(|v_l^{\mathrm{ion}}\rangle\langle v_l^{\mathrm{SO}}| + |v_l^{\mathrm{SO}}\rangle\langle v_l^{\mathrm{ion}}| - \frac{1}{2}|v_l^{\mathrm{SO}}\rangle\langle v_l^{\mathrm{SO}}|\right)\mathbf{L}\cdot\mathbf{S}\langle ls|. \tag{A4}$$

Defining the quantities,

$$Q_1 = \begin{pmatrix} 1 & 0 \\ 0 & \frac{1}{4}l(l+1) \end{pmatrix} Q_2 = \begin{pmatrix} 0 & 1 \\ 1 & -\frac{1}{2} \end{pmatrix}$$

and

$$V_l^0 = \begin{pmatrix} |v_l^{\mathrm{ion}}\rangle \\ |v_l^{\mathrm{so}}\rangle \end{pmatrix},$$

we have

$$V_{\mathrm{NL}} = \sum_l |ls\rangle\underbrace{[{}^tV_l^0 Q_1 V_l^0]}_{V_l^{\mathrm{SR}}}\langle ls| + \sum_l |ls\rangle\underbrace{[{}^tV_l^0 Q_2 V_l^0]}_{V_l^{\mathrm{SO}}}\mathbf{L}\cdot\mathbf{S}\langle ls|. \tag{A5}$$

The Q_1 matrix being diagonal, we can use a Kleinman-Bylander[25] approach with two projectors: the first one is associated with an effective Kleinman-Bylander energy $E_{l,1}^{\mathrm{KB,SR}}=1$ and a semilocal potential v_l^{ion}. The second one is associated with a Kleinman-Bylander energy $E_{l,2}^{\mathrm{KB,SR}} = \frac{1}{4}l(l+1)$ and a semilocal potential v_l^{SO}.

The Q_2 matrix can be diagonalized. Its eigenvalues are $-\frac{1}{4}(1+\sqrt{17})$ and $\frac{1}{4}(-1+\sqrt{17})$ and its eigenvectors, respectively,

$$v_1 = \begin{pmatrix} \frac{1}{4}(-1+\sqrt{17}) \\ 1 \end{pmatrix}, \quad v_2 = \begin{pmatrix} \frac{1}{4}(1+\sqrt{17}) \\ 1 \end{pmatrix}.$$

In this eigenbasis, we have

$$V_l^0 = \begin{pmatrix} -\frac{2}{\sqrt{17}}\left[v_l^{\mathrm{ion}} - \frac{(1+\sqrt{17})}{4}v_l^{\mathrm{SO}}\right] \\ \frac{2}{\sqrt{17}}\left[v_l^{\mathrm{ion}} + \frac{(\sqrt{17}-1)}{4}v_l^{\mathrm{SO}}\right]. \end{pmatrix}$$

We can then use again a Kleinman-Bylander[25] approach with two projectors: the first one is associated with a Kleinman-Bylander energy $E_{l,1}^{\mathrm{KB,SO}}=-\frac{\sqrt{17}}{2}$ and a semilocal potential $-\frac{2}{\sqrt{17}}[v_l^{\mathrm{ion}} - \frac{(1+\sqrt{17})}{4}v_l^{\mathrm{SO}}]$. The second one is associated with a Kleinman-Bylander energy $E_{l,2}^{\mathrm{KB,SO}}=\frac{\sqrt{17}}{2}$ and a semilocal potential $\frac{2}{\sqrt{17}}[v_l^{\mathrm{ion}} + \frac{(\sqrt{17}-1)}{4}v_l^{\mathrm{SO}}]$.

APPENDIX B: CUTOFF SCHEME FOR INTERATOMIC FORCE CONSTANTS

The Fourier interpolation of phonon bands in Pb is complicated by the softenings at several points in the BZ. This gives the bands nonsinusoidal behavior, and higher harmonic contributions appear, i.e., larger long-ranged interatomic force constants. As the longest-ranged IFC which are calculated are not small, by Fourier transforming back we acquire artificial wiggles in the interpolated band structure, in particular near the Γ point. This can be seen in the thin dashed line of Fig. 3, which represents the normally interpolated phonon bands. In this case we have employed the LDA HGH pseudopotential with SO, which compares well with the full GGA TM data with semicore d electrons (thick solid line).

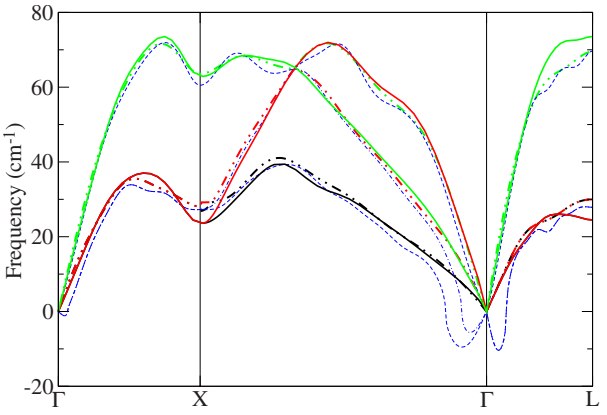

FIG. 3. (Color online) The phonon band structure of lead, with different cutoffs in real space for the interatomic force constants. Thick solid line: phonon bands calculated from the GGA TM SO pseudopotential; thick dot-dashed line: bands for the HGH pseudopotential with a 30 a.u. cutoff on the IFC; and thin dashed line: same with a 85 a.u. cutoff.

This feature of the Fourier transform is analogous to aliasing errors in normal transform theory. The normal solution to this kind of problem is to increase the grid (in our case the density of q points in the irreducible Brillouin zone) until the longest-range IFC decay properly. However, this would entail much heavier calculations.

Using a cutoff in real space for the IFC (neglecting those beyond a certain distance) eliminates the low $-q$ oscillations and gives the thick dot-dashed lines in Fig. 3. As can be seen in the figure, the IFC which are neglected using the cutoff contribute very little to the bulk of the band structure. In this way we have an approximation which gives a good quality band structure without the aliasing effects. Obviously it must be known in advance that the "wiggles" are aliasing and that physical negative modes are not being eliminated.

The cutoff also smooths some of the physical features in the rest of the Brillouin zone, so it must be the subject of a convergence study, at the same time as the sampling grid. We emphasize that relying on a cutoff is not the same as using a coarser BZ sampling: all the q points contribute to improve the convergence of all of the IFC, including the short-ranged ones. Converging the grid density will of course improve the phonon band structure near points that are calculated explicitly, but a controlled use of the IFC cutoff gives similar precision with many fewer wave vectors. Here controlled means ensuring that the negative modes which are eliminated are indeed spurious. An alternative method, intermediate in computational weight between full convergence and our cutoff, has been proposed by Gaál-Nagy[57] adding wave vectors selectively in regions where instabilities appear.

*mjv500@york.ac.uk

[1] S. Baroni, P. Giannozzi, and A. Testa, Phys. Rev. Lett. **58**, 1861 (1987).
[2] X. Gonze, Phys. Rev. B **55**, 10337 (1997).
[3] X. Gonze and C. Lee, Phys. Rev. B **55**, 10355 (1997).
[4] S. Baroni, S. de Gironcoli, A. Dal Corso, and P. Giannozzi, Rev. Mod. Phys. **73**, 515 (2001).
[5] P. Giannozzi, S. de Gironcoli, P. Pavone, and S. Baroni, Phys. Rev. B **43**, 7231 (1991).
[6] S. Baroni, P. Giannozzi, and A. Testa, Phys. Rev. Lett. **59**, 2662 (1987).
[7] D. R. Hamann, X. Wu, K. M. Rabe, and D. Vanderbilt, Phys. Rev. B **71**, 035117 (2005).
[8] L. G. Ferreira, S.-H. Wei, and A. Zunger, Phys. Rev. B **40**, 3197 (1989).
[9] C. J. Pickard and F. Mauri, Phys. Rev. B **63**, 245101 (2001).
[10] D. Sebastiani and M. Parinello, J. Phys. Chem. A **105**, 1951 (2001).
[11] S. Y. Savrasov and D. Y. Savrasov, Phys. Rev. B **54**, 16487 (1996).
[12] C. Lee and X. Gonze, Phys. Rev. B **51**, 8610 (1995).
[13] A. Fleszar and X. Gonze, Phys. Rev. Lett. **64**, 2961 (1990).
[14] G. Deinzer and D. Strauch, Phys. Rev. B **66**, 100301(R) (2002).
[15] M. Lazzeri and F. Mauri, Phys. Rev. Lett. **90**, 036401 (2003).
[16] M. Veithen, X. Gonze, and P. Ghosez, Phys. Rev. Lett. **93**, 187401 (2004).
[17] M. Veithen, X. Gonze, and P. Ghosez, Phys. Rev. B **71**, 125107 (2005).
[18] E. K. U. Gross and R. M. Dreizler, *LDA Density Approximations in Quantum Chemistry and Solid State Physics* (Plenum, New York, 1986), pp. 353–379.
[19] C. L. Kane and E. J. Mele, Phys. Rev. Lett. **95**, 226801 (2005).
[20] M. P. Surh, M.-F. Li, and S. G. Louie, Phys. Rev. B **43**, 4286 (1991).
[21] M. Divis, M. Richter, H. Eschrig, and L. Steinbeck, Phys. Rev. B **53**, 9658 (1996).
[22] C. Hartwigsen, S. Goedecker, and J. Hutter, Phys. Rev. B **58**, 3641 (1998).
[23] G. J. Theurich and N. A. Hill, Phys. Rev. B **64**, 073106 (2001).
[24] X. Gonze *et al.*, Comput. Mater. Sci. **25**, 478 (2002).
[25] L. Kleinman and D. M. Bylander, Phys. Rev. Lett. **48**, 1425 (1982).
[26] X. Gonze *et al.*, Z. Kristallogr. **220**, 558 (2005).
[27] N. Richard, S. Bernard, F. Jollet, and M. Torrent, Phys. Rev. B **66**, 235112 (2002).
[28] D. M. Fritz *et al.*, Science **315**, 633 (2007).
[29] E. D. Murray, S. Fahy, D. Prendergast, T. Ogitsu, D. M. Fritz, and D. A. Reis, Phys. Rev. B **75**, 184301 (2007).
[30] L. E. Diaz-Sanchez, A. H. Romero, and X. Gonze, Phys. Rev. B **76**, 104302 (2007).
[31] L. E. Diaz-Sanchez, A. H. Romero, M. Cardona, R. K. Kremer, and X. Gonze, Phys. Rev. Lett. **99**, 165504 (2007).
[32] J. Bouchet, Phys. Rev. B **77**, 024113 (2008).
[33] D. Vanderbilt, Phys. Rev. B **41**, 7892 (1990).
[34] A. Dal Corso and A. Mosca Conte, Phys. Rev. B **71**, 115106 (2005).
[35] A. Dal Corso, Phys. Rev. B **76**, 054308 (2007).
[36] N. Troullier and J. L. Martins, Phys. Rev. B **43**, 1993 (1991).

[37] P. Hohenberg and W. Kohn, Phys. Rev. **136**, B864 (1964).
[38] W. Kohn and L. J. Sham, Phys. Rev. **140**, A1133 (1965).
[39] X. Gonze, Phys. Rev. A **52**, 1086 (1995).
[40] R. M. Sternheimer, Phys. Rev. **96**, 951 (1954).
[41] X. Gonze and J.-P. Vigneron, Phys. Rev. B **39**, 13120 (1989).
[42] R. M. Pick, M. H. Cohen, and R. M. Martin, Phys. Rev. B **1**, 910 (1970).
[43] A. Fleszar and R. Resta, Phys. Rev. B **34**, 7140 (1986).
[44] L. Kleinman, Phys. Rev. B **21**, 2630 (1980).
[45] G. B. Bachelet and M. Schluter, Phys. Rev. B **25**, 2103 (1982).
[46] X. Gonze, R. Stumpf, and M. Scheffler, Phys. Rev. B **44**, 8503 (1991).
[47] J. P. Perdew, K. Burke, and M. Ernzerhof, Phys. Rev. Lett. **77**, 3865 (1996).
[48] B. N. Brockhouse, T. Arase, G. Caglioti, K. R. Rao, and A. D. B. Woods, Phys. Rev. **128**, 1099 (1962).
[49] A. Y. Liu and A. A. Quong, Phys. Rev. B **53**, R7575 (1996).
[50] H. J. Monkhorst and J. D. Pack, Phys. Rev. B **13**, 5188 (1976).
[51] M. J. Verstraete and X. Gonze, Phys. Rev. B **74**, 153408 (2006).
[52] W. Kohn, Phys. Rev. Lett. **2**, 393 (1959).
[53] L. Pisani and R. Valenti, Phys. Rev. B **71**, 180409(R) (2005).
[54] C. Audouze, F. Jollet, M. Torrent, and X. Gonze, Phys. Rev. B **73**, 235101 (2006).
[55] C. Audouze, F. Jollet, M. Torrent, and X. Gonze, Phys. Rev. B **78**, 035105 (2008).
[56] L. A. Hemstreet, C. Y. Fong, and J. S. Nelson, Phys. Rev. B **47**, 4238 (1993).
[57] K. Gaál-Nagy, Phys. Rev. B **77**, 024309 (2008).